The Journal of Chemical Physics

Spontaneous polarization of thick solid ammonia films

Cite as: J. Chem. Phys. **153**, 124707 (2020); https://doi.org/10.1063/5.0017853
Submitted: 10 June 2020 . Accepted: 03 September 2020 . Published Online: 24 September 2020

Roey Sagi, Michelle Akerman, Sujith Ramakrishnan, and Micha Asscher

The Journal of Chemical Physics ARTICLE scitation.org/journal/jcp

Spontaneous polarization of thick solid ammonia films

Cite as: J. Chem. Phys. 153, 124707 (2020); doi: 10.1063/5.0017853
Submitted: 10 June 2020 • Accepted: 3 September 2020 •
Published Online: 24 September 2020

Roey Sagi, Michelle Akerman, Sujith Ramakrishnan, and Micha Asscher[a)]

AFFILIATIONS

Institute of Chemistry, Edmond J. Safra Campus, Givat-Ram, The Hebrew University of Jerusalem, Jerusalem 9190401, Israel

[a)]Author to whom correspondence should be addressed: micha.asscher@mail.huji.ac.il

ABSTRACT

Ammonia molecules have an important role in the radiation-induced chemistry that occurs on grains in the cold interstellar medium and leads to the formation of nitrogen containing molecules. Such grains and surfaces are primarily covered by water ices; however, these conditions allow the growth of solid ammonia films as well. Yet, solid ammonia know-how lags the vast volume of research that has been invested in the case of films of its "sibling" molecule water, which, in the porous amorphous phase, spontaneously form polar films and can cage coadsorbed molecules within their hydrogen-bonded matrix. Here, we report on the effect of growth temperature on the spontaneous polarization of solid ammonia films (leading to internal electric fields of ~10^5 V/m) within the range of 30 K–85 K on top of a Ru(0001) substrate under ultra-high vacuum conditions. The effect of growth temperature on the films' depolarization upon annealing was recorded as well. By demonstrating the ability of ammonia to cage coadsorbed molecules, as water does, we show that temperature-programmed contact potential difference measurements performed by a Kelvin probe and especially their temperature derivative can track film reorganization/reconstruction and crystallization at temperatures significantly lower than the film desorption.

I. INTRODUCTION

The study of solid ammonia films is relevant to astrochemistry and astrophysics, since ammonia is among the most abundant molecules in the interstellar medium (ISM), with an abundance of 1%–10% with respect to that of water,[1] and can be found in molecular clouds (MC) and in star forming and circumstellar regions.[2,3] Ammonia has also been detected on planetary bodies in our solar system—on planets,[4–7] their atmospheres,[8–10] satellites,[4,5,11–13] asteroids, and comets.[14] The low temperatures characterizing these extraterrestrial environments (10 K–100 K) allow the growth of pure or mixed icy layers via condensation of gas-phase molecules. Ice growth on top of dust grains is presumed to accelerate their gravitational collapse and to increase their sticking probability to form larger aggregates, processes that eventually lead to the formation of pre-stellar cores and planetesimals.[15–17] Moreover, such films are subject to continuous photo- and radiation-induced chemistry, where ammonia is presumed to be an important precursor for the formation of nitrogen-bearing molecules detected on interstellar icy grains.[18–23] In addition, ammonia detection within the icy surfaces of planetary bodies in our solar system suggests geophysical activity[24] and the presence of liquid water at their subsurface.[25] Furthermore, due to its resemblance to water, ammonia may also be important in the study of hydrogen bonding and defect-induced proton mobility[26–28] and to the study of charged particles solvation within ices.[29,30]

In this work and in a parallel study,[31] we demonstrate the spontaneous polarization of solid ammonia films and contribute to the general understanding of this phenomenon, previously observed and reported for the case of amorphous solid water (ASW). ASW films demonstrate a strong growth temperature (T_{gr}) dependence on the evolution of polarization, which mostly derives from the T_{gr} dependent film porosity, due to dipole orientation normal to the substrate on the pore walls. Both water and ammonia molecules share many properties; among them, their tetrahedral structure (including the electron lone pairs) and the ability to form hydrogen bonding. Both molecules are polar, with a gas phase dipole moment of 1.85 D and 1.42 D for water and ammonia, respectively. In the solid phase, the potential of water ices to form polar (amorphous) films has drawn considerable attention throughout the past decades.

This is in contrast to ammonia, whose important astrochemical role has only recently been recognized and, so far, this possibility was ignored (excluding a brief statement in the work of Kutzner,[32] although without any demonstration, and the very recent publication by Cassidy *et al.*[33]). Hence, it is of interest to explore and compare the macroscopic nature of polarization of the two molecular ice systems. Contact potential difference change (ΔCPD) measurements were performed for both ASW (presented in a separate publication) and ammonia during the growth of thick films condensed on Ru(0001). We examined the effect of substrate temperature on ΔCPD that develops between the film/vacuum and the film/substrate interfaces. ΔCPD is further *in situ* monitored, while these films are subsequently being annealed.

Thick films of solid ammonia were studied so far mostly by infrared measurements,[34–38] associating the IR bands with the structure and phase of the ammonia films. Changes in the work function as a result of and during the growth of submonolayer coverages were indirectly recorded.[39–41] Yet, neither the macroscopic net polarization of thick ammonia films nor continuous CPD measurements during the growth of solid ammonia layers and during film annealing had been reported previously. Such measurements are of interest because they provide new information on the macroscopic morphology and dielectric properties of the icy film, revealing how they are influenced by the substrate temperature during film growth or upon temperature modifications. This report focuses on the spontaneous polarization of solid ammonia films during their growth as well as on the structural changes and phase transitions these films undergo while annealed by employing ΔCPD measurements.

II. EXPERIMENTAL METHODS

Hundreds of monolayers (ML)-thick solid ammonia films were grown under ultra-high vacuum (UHV) conditions (base pressure of $<2 \times 10^{-10}$ Torr) on a $8 \times 8 \times 2$ mm^3 Ru(0001) substrate attached to a closed-cycle He cryostat (Janis) by two 0.4 mm diameter Ta wires spot-welded to the crystal's top and bottom edges and to two 2.8 mm Ta rods connected to the cryostat. Temperature readings of the ruthenium sample are acquired by a K-type thermocouple spot-welded to one side of the substrate, providing accuracy of ±0.5 K. A LabVIEW algorithm enables reading of the temperature and the controlled resistive heating/cooling of the substrate at linear rates in the range of 0.5 K/s–10 K/s. The cryostat can cool the sample down to a base temperature of 30 K, with additional capability to modify the sample's temperature by utilizing a Si diode and a 50 Ω cartridge heater attached at the bottom of the cryostat. This together with its designated temperature controller (LakeShore 335) enabled accurate base temperature control in the range of 30 K–300 K. The ruthenium surface is daily sputter-cleaned by 800 eV Ne^+ ions for 12 min, followed by annealing to 1450 K for 3 min. The chamber is equipped with a quadrupole mass spectrometer (QMS, RGA-300, Stanford Research Systems) and a Kelvin probe (KP–S, Besocke-Delta-Phi) for the performance of continuous ΔCPD measurements. Coupling to the controlled heating enables temperature-programmed desorption (ΔP-TPD) measurements. Continuous monitoring of the surface work function change (ΔCPD) enables us to record ΔCPD, while rearrangements of the adsorbates take place prior to any desorption (ΔΦ-TPD or temperature-programmed ΔCPD measurements, TP-ΔCPD). Moreover, the latter's derivative spectrum, d(ΔCPD)/dT, provides a unique perspective on the polarization of the films.[42–47] The UHV chamber is further equipped with an electron source (1 eV–2000 eV; ELG-2, Kimball Physics) and a mini-Auger analyzer (LK technologies, attached via a 2.75″ flange) for determining the surface cleanliness. Ammonia (NH_3, Sigma-Aldrich, 99.99+%) vapor was introduced by backfilling the UHV chamber through a high-precision leak valve, ensuring homogeneous coverage on the sample and its cold surroundings. The exposure of a 1 ML-thick film (calculated in langmuir units, L, where 1 L = 10^{-6} Torr · s) was derived from the emergence onset of the ammonia multilayer desorption peak while performing exposure dependent ΔP-TPD measurements. One monolayer of NH_3 is equivalent to the exposure of 0.15 L (without ion gauge corrections).

III. RESULTS AND DISCUSSION

A. The first layers of ammonia on Ru(0001)

Thick solid ammonia films have not been studied so far by employing ΔCPD measurements, and our first aim is to lay some of the foundations required for our analysis of the ammonia system. Molecular chemisorption on metal surfaces alters the surface charge distribution. Subsequent annealing to sufficiently high temperatures will eventually lead to desorption of the adsorbates from the surface, restoring its initial state assuming that no dissociation fragments remained strongly attached to the surface. Continuous ΔCPD measurements during the growth of the first layers and during a programmed heating process will monitor and respond to these events. TP-ΔCPD measurements and, more specifically, their temperature derivative [d(ΔCPD)/dT] spectra can be compared to standard ΔP-TPD measurements[43] and to add further information regarding events occurring at temperatures significantly below the desorption onset. Standard ΔP-TPD measurements provide information on the kinetics and binding energies of adsorbates to the substrate (in the submonolayer regime) and on intermolecular interactions.[39,46,48–51] As a complementary tool, TP-ΔCPD data can introduce further information on macroscopic molecular orientation and morphological changes that take place in response to film warming. A comparison between the two techniques, as shown in Fig. 1(a), is essential because it may assist us identifying features observed in the case of thick films, where standard ΔP-TPD cannot introduce new features above a few to tens of monolayers (multilayer).

Ammonia adsorption on transition and noble metal surfaces has been investigated by various tools,[30,39–41,52–57] including standard ΔP-TPD. These measurements reveal minor differences between substrates, mainly in peak positions. Desorption profiles from these surfaces share a broad high-temperature desorption peak attributed to the first monolayer. The broadening is associated with dipole–dipole repulsive interactions, forcing the dipoles to reorient in order to reduce the system's free energy, consequently lowering the effective activation energy for desorption as coverage as coverage increases,[39] due to desorption from different adsorption sites-atop or threefold hollow[57] or even due to desorption of hydrogen-bonded

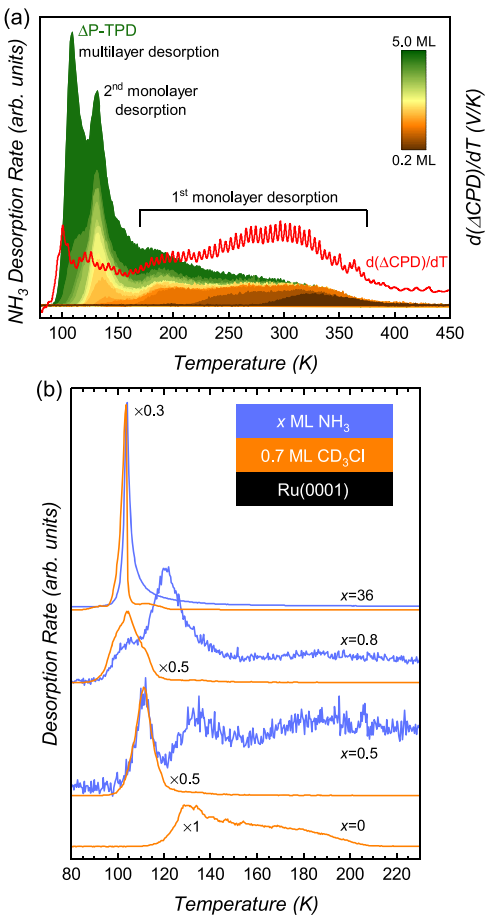

FIG. 1. The first layers of ammonia on the Ru(0001) surface. (a) Temperature-programmed desorption (ΔP-TPD) spectra of ammonia (atomic mass to charge ratio, m/z = 17) and submonolayer to multilayer coverages [up to 5 monolayers (ML); heating rate of 4 K/s], demonstrating its similarity to the temperature derivative spectrum of temperature-programmed contact potential difference change (TP-ΔCPD) measurements (shown in Fig. S1 of the supplementary material), d(ΔCPD)/dT, of multilayer thick ammonia film (in red). (b) ΔP-TPD measurements (1 K/s heating rate; relative scaling is noted next to each curve) of 0.7 ML CD_3Cl (53 m/z; in orange) adsorbed directly on the ruthenium substrate and capped by different ammonia coverages (not to scale; in blue), demonstrating the ability of ammonia to compress and to cage coadsorbed species, eventually desorbing as a "volcano" together with the ammonia multilayer at 110 K.

molecules from dimers.[56] These measurements also share two sharp features at lower temperatures ascribed to the desorption of the second monolayer and the multilayer. Figure 1(a) demonstrates that Ru(0001) is not exceptional, with ammonia coverage dependent ΔP-TPD spectra (atomic mass to charge ratio, m/z, of 17; coverage of 0.2 ML–5.0 ML and heating rate of 4 K/s; colored scale). The first monolayer desorbs in the temperature range of 150 K–390 K (with two local maxima at 203 K and 310 K). The second monolayer and the multilayer exhibit narrower peaks where the onsets for desorption are seen at 110 K and 80 K, respectively. The maximum desorption rate of the second monolayer is obtained at 131 K, whereas the multilayer exhibits a zero-order kinetics. A corresponding d(ΔCPD)/dT spectrum (red line; 1 K/s heating rate) of 40 ML-thick ammonia film follows the trends of the standard ΔP-TPD profile [the TP-ΔCPD profile is shown in Fig. S1(a) of the supplementary material]. It exhibits a broad high-temperature feature attributed to the first monolayer realignment and desorption and the two low-temperature peaks of the second monolayer and the multilayer.

Essential to our analysis is the ability of ammonia to compress and cage pre- or coadsorbed polar and nonpolar molecules inside structural pockets. This is analogous to the behavior of water and is evident by the abrupt release of these molecules upon temperature increase (the "molecular volcano"). The caging phenomenon is well-documented for water;[58–60] however, it has never been previously demonstrated for any other molecular film, ammonia in particular, which obviously is a natural candidate for comparison. This is presented in Fig. 1(b). Methyl chloride is an excellent demonstrator because it has a broad desorption profile when adsorbed on Ru(0001), very similar to that of ammonia [see Ref. 47 and Fig. S1(b) of the supplementary material]. Thus, it can demonstrate the ammonia's capability of caging. A fixed 0.7 ML CD_3Cl coverage was deposited on top of the clean ruthenium substrate. Subsequently, increasing levels of ammonia coverages were deposited on top [see the inset of Fig. 1(b)]. ΔP-TPD measurements tracked the desorption profiles of the two species (CD_3Cl in orange and NH_3 in blue, not to scale). The broad submonolayer desorption peak of CD_3Cl seen without any ammonia overlayer (bottom) is significantly compressed when the ammonia is significantly compressed when the ammonia submonolayer coverage increases and its peak gradually shifts to lower temperatures (from 130 K without any ammonia capping down to 110 K with 0.5 ML of subsequently adsorbed ammonia and further to 103 K with ammonia multilayer on top). The profiles of both species indicate the formation of methyl chloride multilayer islands. This we believe is the compression stage, where the two-dimensional film contracts to form three-dimensional structures, whether they are mixed with the ammonia or not is an open question, since the ammonia molecules interact with both the adsorbed CD_3Cl molecules and the substrate. At multilayer coverages of ammonia, the CD_3Cl molecules are encapsulated.[58] Therefore, when capped by the 36 ML-thick ammonia film, it desorbs together with the ammonia multilayer in the temperature range of 94 K–106 K (FWHM of only 3 K), typical for the so-called "volcano desorption" phenomenon. These two building blocks are of great importance on their own and will further serve us here.

The growth of thick ammonia films on the Ru(0001) substrate was performed via backfilling the UHV chamber with room temperature ammonia vapor adsorbed on the substrate at temperatures in the range of 30 K–85 K at a fixed growth rate of 7 ML/s while continuously recording the ΔCPD. In Fig. 2(a), ΔCPD profiles measured during the growth of 3300 ML-thick films at different growth temperatures are shown. When the exposure approached the desired value, the leak valve was closed and the ammonia vapor pressure dropped down, and at sufficiently low pressure, the substrate was cooled to 30 K.

An initial T_{gr} independent sharp drop of the ΔCPD profile down to a minimum value of −3.4 V is observed. This value is obtained at ammonia layer thickness of ~30 ML. The saturation of the first monolayer on Ru(0001) occurs at a coverage of

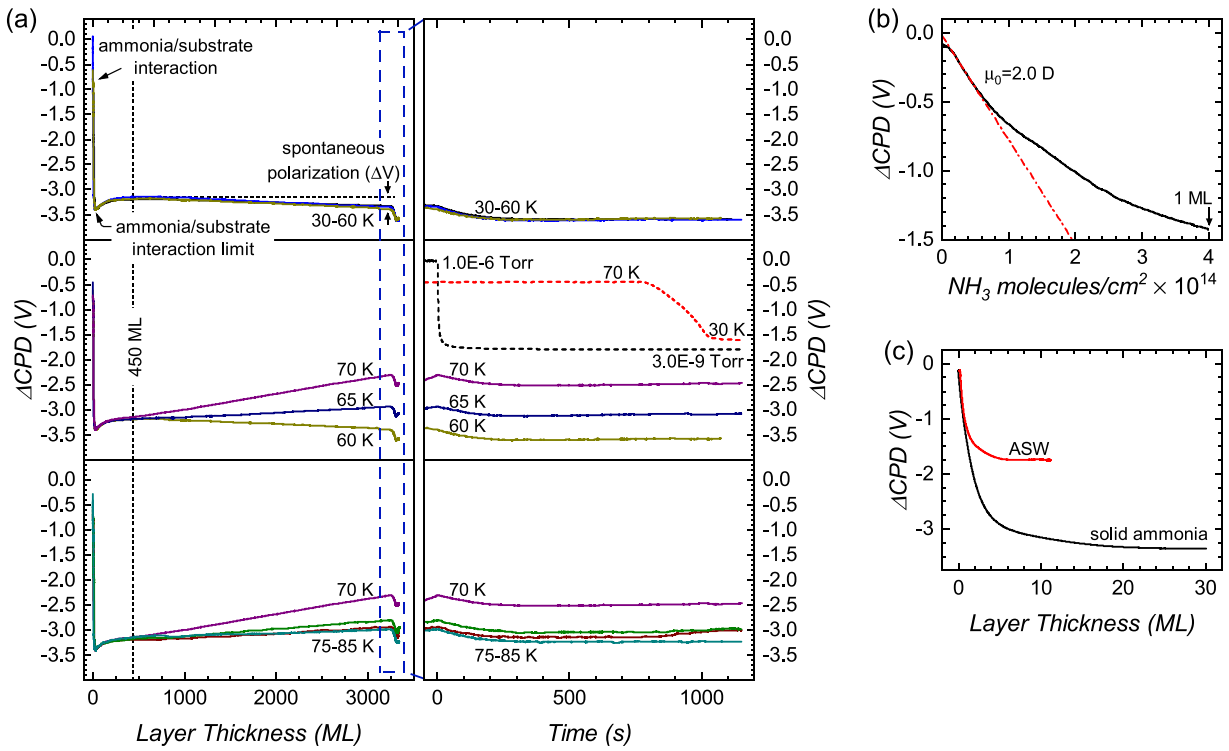

FIG. 2. ΔCPD curves during the growth of 3300 monolayers (ML)-thick solid ammonia films on top of the Ru(0001) substrate at temperatures in the range of 30 K–85 K (denoted by T_{gr}). (a) The left-hand side panels are ΔCPD measurements recorded during the growth of ammonia layers at the indicated temperatures; the blue dashed rectangle denotes the exposure termination (leak-valve closure; initiates the observed voltage-drop). Films were then cooled down to 30 K. Right-hand side panels of (a): ΔCPD-versus-time curves following the leak-valve closure (pressure reduction at t = 0). A typical chamber's pressure-drop profile and a representative substrate temperature profile of a film grown at 70 K and then cooled down to 30 K are demonstrated in the middle-right panel by the black and red dashed lines, respectively. (b) ΔCPD during adsorption of ammonia's first monolayer vs its surface density. The coverage of a complete (ordered) ammonia monolayer on Ru(0001) is 0.25 [with 2 × 2 overlayer structure (see Ref. 39) and the Ru(0001) surface density is 1.57×10^{15} atoms/cm^2]. (c) A comparison between ΔCPD profiles during the growth of both ammonia and amorphous solid water (ASW) multilayers until the ΔCPD minimum is established.

~0.25 (NH_3/Ru), presenting a 2 × 2 overlayer structure, i.e., surface density of 4.0×10^{14} molecules/cm^2 (recorded by LEED measurements performed by Benndorf and Madey[39]). The first monolayer contributes ~40% of the −3.4 V minimum obtained at 30 ML, implying a strong interaction of the first ammonia layers with the substrate.

At the limit of zero coverage, the dipole moment is independent of the adsorbate surface density, and thus, one may ignore dipole–dipole interactions with the nearest neighbors and apply the following Helmholtz equation:

$$\Delta CPD = \frac{N\mu}{\varepsilon_0}, \tag{1}$$

where N is the surface density of the ammonia molecules, ε_0 is the vacuum permittivity (8.85×10^{-12} C V^{-1} m^{-1} or, for convenience, 2.66×10^{14} D V^{-1} cm^{-2}, where 1 D = 3.33×10^{-30} C m), and μ is the adsorbates effective dipole moment, modified by interaction with the substrate. Since the dipole is density independent, it can be extracted directly from the slope of the (initially) linear ΔCPD vs molecular density profile seen at this coverage range [see Fig. 2(b)] according to Eq. (1). This calculation yields a dipole moment value of 2.0 D, in agreement with the value reported by Benndorf and Madey.[39] The dipole moment enhancement relative to the gas-phase value of 1.42 D is the result of the bonding nature of ammonia molecules to the ruthenium surface and the dipole orientation with respect to the substrate. Ammonia bonds to the surface via the nitrogen atom, promoting charge-transfer from the nitrogen lone-pair electrons to the metal.[39] Moreover, at this coverage range, ammonia molecules are aligned normal to the substrate.[39,56] In response, the metal substrate forms an image potential within it, which further contributes to the dipole moment increase.[61]

At higher coverages, up to the completion of the first monolayer, the adsorbed molecules reduce their z-direction dipole alignment, responding to dipole–dipole interactions; however, they do wet the surface, forming a compact first layer.[39] This further contributes to the establishment of the ΔCPD minimum. The upper-layer molecules contribute to the measured ΔCPD as well, however, with a gradually decreasing influence. At thicker films (above 30 ML), this stops from playing a role, indicating the limit of interaction of the stacked ammonia layers with the substrate. Similar

minimum was obtained for water, however, at lower thickness (10 ML) and with smaller ΔCPD voltage drop [−1.75 V, see Fig. 2(c)], implying a stronger interaction of the ammonia molecules with the substrate. This is also evident from the much broader first monolayer desorption profile that ammonia presents [Fig. 1(a)], indicating that an increased charge transfer from the ammonia to the ruthenium takes place. Additionally, ammonia presents an enhanced alignment normal to the substrate and a better wetting than water (at the same coverage), which at low coverages forms almost planar rings,[62] practically commensurate with the hexagonal 0001 plane of the substrate. At higher coverages, adsorbed water molecules cluster to form three-dimensional islands, indicating that their interaction with the substrate is weaker.

B. Polarization of thick solid ammonia films

The initial ΔCPD minimum of −3.4 V obtained at 30 ML is followed by a T_{gr} independent net orientation change (the ΔCPD increases with thickness) in the ammonia layer thickness range of 30 ML–450 ML. Further growth (above 450 ML) leads to another break, this time T_{gr} dependent, revealing three different T_{gr} regimes. All films grown below 60 K exhibit practically identical decrease in the ΔCPD, i.e., polarization flipping. At some temperature between 60 K and 65 K, the net-orientation does not flip and it maintains a positive slope after the break at 450 ML. The ΔCPD slope further increases with T_{gr}. Films grown at 70 K present the highest slope, with lower but still positive slopes at $T_{gr} > 70$ K.

Further development of the Helmholtz equation for thick films will give a simplistic description of the voltage difference evolved by the following analog to a parallel-plate capacitor behavior:[32]

$$\Delta V = \frac{M_{(T)}\tilde{\mu}_{z(T)}}{A\varepsilon_0\varepsilon_{(T)}}, \tag{2}$$

where M is an integer representing the effective number of dipoles with some "up" orientation ($M = N_\uparrow - N_\downarrow$, where $N_{\uparrow,\downarrow}$ is the total number of dipoles, either with net "up" or "down" orientation, respectively). $\tilde{\mu}_z$ is the average z-axis (normal to the substrate surface) molecular dipole component, A is the substrate area, and $\varepsilon_{(T)}$ is the relative permittivity (dielectric constant) of the film (3.4 at low temperatures,[32,63] very similar to that of water films,[32,64,65] with $\varepsilon_{(T)} = 3.2$). Note that the potential develops within the film, ΔV is offset by the film/substrate interaction, and its slope is opposite in sign in comparison to the measured ΔCPD during film growth (see also Sec. V of the supplementary material). The internal electric field should not contain any lateral contributions, only the z-component (due to symmetry considerations), which can be calculated according to

$$E_z = \frac{d(\Delta CPD)}{dz}. \tag{3}$$

Yet, to properly calculate the field, one must translate the thickness expressed in monolayers to actual length scales. Although it seems straightforward, care should be taken because our notation of thickness assumes a compact film. This is not the case, since the films are porous below 60 K.[37] In fact, the films are not of equal thickness but of equal mass—to that of a compact film. The internal electric field can be calculated from the linear trend of each of the ΔCPD vs thickness profiles in the range of 450 ML–3300 ML by the following term (see Sec. V of the supplementary material):

$$E_z = \frac{d(\Delta CPD)}{dz} \cong \frac{\Delta(\Delta CPD)}{\Delta(\#ML)s\rho_c/\rho}, \tag{4}$$

where s is the interlayer spacing (i.e., the monolayer thickness is 2.54 Å,[66] assuming that it is equal to that of crystalline ammonia). ρ_c and ρ are the compact and porous film densities, respectively. The values for the T_{gr} dependent density are taken from the work of Satorre *et al.*[37] (see also Table SII of the supplementary material; $\rho_c = 0.89$ g/cm^3). We then calculate the growth temperature dependent internal electric field in the T_{gr} range of 30 K–85 K. This is shown in Fig. 3. These calculations result in internal electric fields in the range of −4.6 to 12.3 × 10^5 V/m. From the linear correlation between the polarization and the electric field, one can calculate the average z-component of the dipole moment, $\tilde{\mu}_z$. $\tilde{\mu}_z$ can be expressed as follows:[67]

$$\tilde{\mu}_z = \varepsilon_0\Omega\frac{d(\Delta CPD)}{dz}, \tag{5}$$

where Ω is the molecular volume (19.56 Å^3,[68] an approximation of the van der Waals molecular volume). The calculated values of $\tilde{\mu}_z$ are in the range of 0.9 × 10^{-5} D–6.4 × 10^{-5} D. More interesting is the average level of dipole orientation, $\tilde{\mu}_{z(T)}/\tilde{\mu} = \langle\cos\theta\rangle$, where θ is the angle between the total dipole and the z-direction, normal to the surface. However, for this, one should know the absolute magnitude of $\tilde{\mu}$. This is an unknown quantity and we will adopt

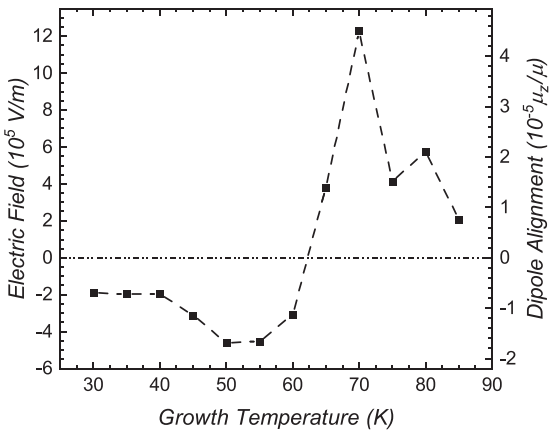

FIG. 3. Internal electric field and the average dipole alignment (upper limit) inside 3300 ML-thick solid ammonia films. The internal field and the average dipole orientation are calculated according to Eqs. (4) and (5), respectively. Gas-phase value of the ammonia molecule's dipole moment was used for the calculation of the dipole orientation, serving as an upper limit. The dipole flipping is apparent in both the field and the dipole alignment when they change their sign (from negative to positive values) at T_{gr} between 60 K and 65 K.

instead the gas-phase value, estimating an upper limit for the actual alignment. This assumption can be justified, since one expects the dipole to increase, mostly due to the ability to form hydrogen-bonds (similar to the case of condensed water and in contrast to expected values from other models that neglect such interactions, see Refs. 69 and 70, respectively). The upper limit alignment percentage, in the range of 0.7×10^{-3}%–4.5×10^{-3}%, is also depicted in Fig. 3 (values can be found in Table SII of the supplementary material). The temperature dependence of the dipole moment orientation along the z-direction is generally described through a Langevin function;[67] however, this monotonic function cannot describe both the polarization flipping seen at 60 K–65 K and the multiple trend shifts. Similar behavior except for the change in sign was demonstrated by Plekan *et al.*[71] for *cis*-methyl formate deposited under similar conditions. These researchers have formulated a broader representation of the total local field, where the measured spontaneous field is only one parameter in a *spontelectric* model. Observation of the first derivative of the Langevin function under the assumption of low local electric fields can partially reconstruct the trend shifts. Yet, this description does not consider the strong hydrogen-bonding ammonia molecule form compared to the electrostatic forces[28] and a similar quantitative analysis we could not manage to perform here. Nonetheless, a test of the spontelectric nature of solid ammonia films was very recently reported by Cassidy *et al.*,[33] who examined much thinner films (~30 ML) following vacuum ultraviolet (VUV) absorbance, mostly of wavelengths near 125 nm, which ionize the condensed ammonia molecules. They have extracted fields two orders of magnitude higher than those reported here. While it is difficult to account for the origin of these large discrepancies, we postulate that this may be the result of electron stabilization/solvation by surrounding dipoles.[72]

The growth of the films stops when the ammonia vapor pressure drops (when closing the leak valve). This initiates a decay of the ΔCPD [see inside the blue dashed rectangle in left-hand side panels of Fig 2(a), after 3300 ML of Fig. 2(a)]. Right-hand side panels of Fig. 2(a) show the ΔCPD profile vs time from the moment the pressure drops (t = 0; typical pressure vs time profile is shown in black dashed line in the middle-right panel). While the pressure decreases instantly, the corresponding decay of the ΔCPD is significantly slower. This behavior correlates with a relaxation process the films undergo, i.e., an attempt of the system to reduce its free energy, perhaps by healing of defect sites that initiates a reduction of the internal field, which in turn leads to a lower degree of alignment of the dipoles. This self-limiting process eventually saturates. Such a process is expected to be thermally activated; however, all films show similar voltage decay between 30 K and 85 K.

Additionally, the subsequent substrate cooling [begins at t ≈ 800 s when the vacuum recovers; an example of the cooling profile is shown by the red dashed line in the middle-right panel of Fig. 2(a)] seems to have no impact on the polarization. This may indicate that the observed polarization is not the result of a pyroelectric effect. Moreover, these results are actually characteristic of materials known as "*spontelectric*."[73] Such materials—polar molecular films, e.g., methyl formate, condensed on a cold substrate, reveal a similar growth temperature dependence of the internal electric field and the dipole alignment, including the different voltage (ΔCPD) evolution trends seen at different growth temperature regimes, as well as the relaxation process at growth termination.

C. Annealing thick solid ammonia films

Once grown, the thick ammonia films were heated at a rate of 1 K/s until their full desorption at 400 K. TP-ΔCPD measurements and their corresponding d(ΔCPD)/dT spectra are presented in Fig. 4. The trends observed during films' growth are also apparent in both the TP-ΔCPD and the d(ΔCPD)/dT profiles. All films reveal three main features in the temperature range of 30 K–180 K. TP-ΔCPD profiles [Fig. 4(a)] demonstrate the evolution of a broad maximum between 105 K and 160 K, which peaks at 155 K. This is followed by a mild voltage decrease up to 170 K and increases again at higher temperatures. The TP-ΔCPD profiles also show a lower intensity, broad low temperature maximum that shifts to higher temperatures with T_{gr} in the range of 30 K–60 K [Fig. 4(a), curves (a)–(d)]. For films grown at 30 K [Fig. 4(a), curve (a)], this local maximum is obtained at 65 K. The peak emergence (assigned to the depolarization of the film while the voltage rises) and its subsequent decay (regaining polarization) span the entire temperature range of 30 K–105 K. For T_{gr} = 50 K (see Fig. S2 of the supplementary material), the peak coincides with the higher temperature voltage (ΔCPD) ramp, prior to the appearance of any decay. An inflection point is formed this way that shifts to higher temperatures with T_{gr}. This feature disappears when films are grown at 65 K and above [Fig. 4(a), curves (e)–(h)]. Simultaneously, a minimum emerges around 113 K. These features can further be analyzed by monitoring the d(ΔCPD)/dT spectra [Fig. 4(b)], which represent the rate of polarization change upon heating.

The d(ΔCPD)/dT spectra reveal a maximum at 115 K and a minimum at 160 K. This is common to all growth temperatures. According to the analysis of Fig. 1(a), these peaks are attributed to the multilayer and the onset of ammonia monolayer desorption, respectively (a full-scale, up to 400 K, TP-ΔCPD measurement and its temperature derivative of thick ammonia film are shown in Fig. S3 of the supplementary material). Note that upon annealing, ΔCPD at 160 K equals −2.8 V, a 1.3 V higher than the ΔCPD value recorded during the growth of the first monolayer [~−1.5 V, Fig. 2(b)]. This significant difference may be associated with the modification of the first monolayer interaction with the substrate, i.e., increased alignment of the dipoles normal to the substrate, either in response to the stacking of layers above or due to the increased thermal energy available upon annealing. STM studies of the first monolayers of ASW on the Ru(0001) surface performed by Maier *et al.*[62] have shown that the growth of higher layers impose the restructuring of the first water monolayer to commensurate with the 0001 plane of the ruthenium substrate (forming a planar layer of hexamers). As was mentioned before and unlike the planar structure of water, first monolayer ammonia molecules tend to be vertically aligned.[39,56] Ordering of the first monolayer due to the stacking of higher layers or due to film crystallization upon annealing may lead to stronger interaction with the substrate, mostly due to improved and thus increased image potential within the metal, which is expected to result in an increased ΔCPD.

A direct comparison of the d(ΔCPD)/dT spectra with a standard ΔP-TPD measurement cannot explain the low temperature features because the onset for ammonia desorption is observable only above 80 K (see Fig. 1 and Fig. S4 of the supplementary material). One can overcome this by utilizing ammonia's ability to trap other species within its matrix, as was demonstrated in Fig. 1(b). Although

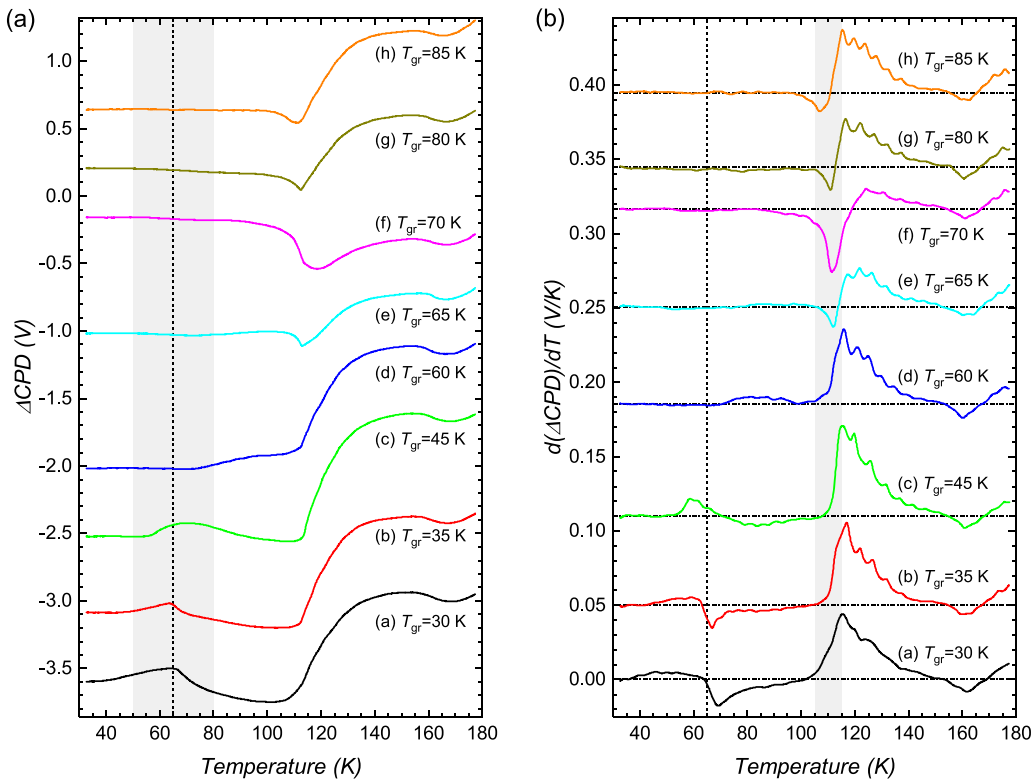

FIG. 4. Solid ammonia films responding to temperature modifications. TP-ΔCPD spectra (a) and their temperature derivative, d(ΔCPD)/dT (b), of 3300 ML-thick ammonia films grown at the indicated temperatures and subsequently cooled down to 30 K prior to their annealing at a heating rate of 1 K/s. All plots except that at T_{gr} = 30 K are arbitrarily offset (in the *y*-axis) for clarity. Horizontal dashed-dotted lines in (b) mark d(ΔCPD)/dT = 0.

an excellent model, the methyl chloride molecule is neither unique nor will be useful for that purpose, since it strongly interacts with ammonia and will not desorb at the relevant (low) temperature range. A better strategy is to adsorb low coverage of weakly interacting atoms on top of the films, thus expected to desorb upon any minor surface modification. A suitable adsorbate is the inert Kr atom, which weakly binds to surfaces. The weak interaction of Kr with the ammonia film surface will lead to its release at low temperatures upon annealing unless it is trapped within the molecular matrix. In this case, it will either desorb together with the multilayer or upon any reconstruction that may occur in the film at a lower temperature, similar to that experienced with water.[31,60]

So far, we have addressed the ammonia films only as solids without specifying any information regarding their state, for instance, their phase or morphology. In the relevant temperature range (30 K–85 K), the film morphology varies in porosity[37] and can either be amorphous or crystalline.[36–38] Despite the limited temperature range (dictated by the onset for multilayer desorption), the relatively low level of polarization, and the limited literature, which makes the analysis of the ammonia system more complicated, our data indicate that one can track the morphological changes and phase transitions. Figure 5 depicts a Kr ΔP-TPD measurement (84 m/z; orange solid line) at Kr coverage equivalent to 3 ML (as defined on the bare ruthenium) deposited on top of the 3300 ML-thick ammonia film, both deposited at 30 K. This is then compared to the TP-ΔCPD measurement of an identical ammonia film (in blue solid line) and with its d(ΔCPD)/dT spectrum (blue dashed line). The ΔP-TPD profile shows three Kr desorption peaks—at 52 K, 65 K, and 115 K. The ammonia multilayer desorption peak observed at 115 K is well represented in both the Kr ΔP-TPD (Kr atoms desorb together with the ammonia multilayer) and the d(ΔCPD)/dT spectra.

The small Kr desorption peak observed at 65 K (magnified 100-fold) corresponds to the 65 K peak seen in the ammonia TP-ΔCPD measurement. We assign this to crystallization of the amorphous ammonia film to its cubic crystalline phase. Zheng and Kaiser[38] have reported crystallization of amorphous ammonia to occur at 57 K, 8 K lower than our assignment. They have also reported that by adding 1% of water into the solid ammonia film, a shift of the phase transition temperature to 65 K is observed. However, this is unlikely to be the case here because of the experimental conditions under which the measurements were conducted: base pressure $<2.0 \times 10^{-10}$ Torr in the UHV chamber and high-vacuum base pressure in the prechamber reservoir (manifold) before it was introduced together with the ammonia vapor. Just like ΔP-TPD measurements, the TP-ΔCPD profiles and their temperature derivative strongly depend

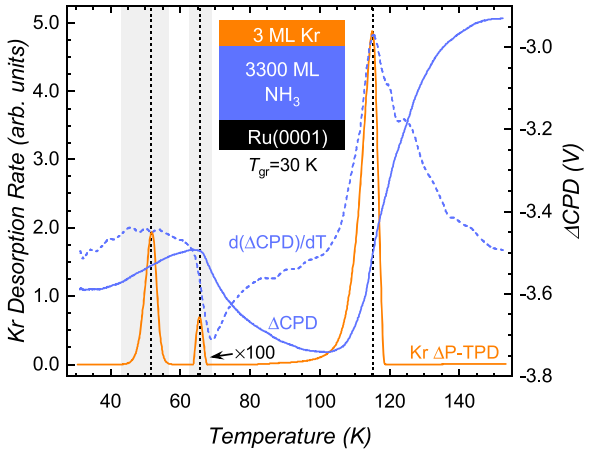

FIG. 5. Analysis of the TP-ΔCPD and d(ΔCPD)/dT spectra by Kr ΔP-TPD. TP-ΔCPD profile (blue solid line) and its temperature derivative (blue dashed line) of 3300 ML-thick solid ammonia film grown at 30 K. A 3 ML-thick Kr layer was deposited at 30 K on top of an equivalent ammonia film; its ΔP-TPD spectrum (84 m/z, orange solid line) is shown for comparison. In both measurements, the heating rate was 1 K/s.

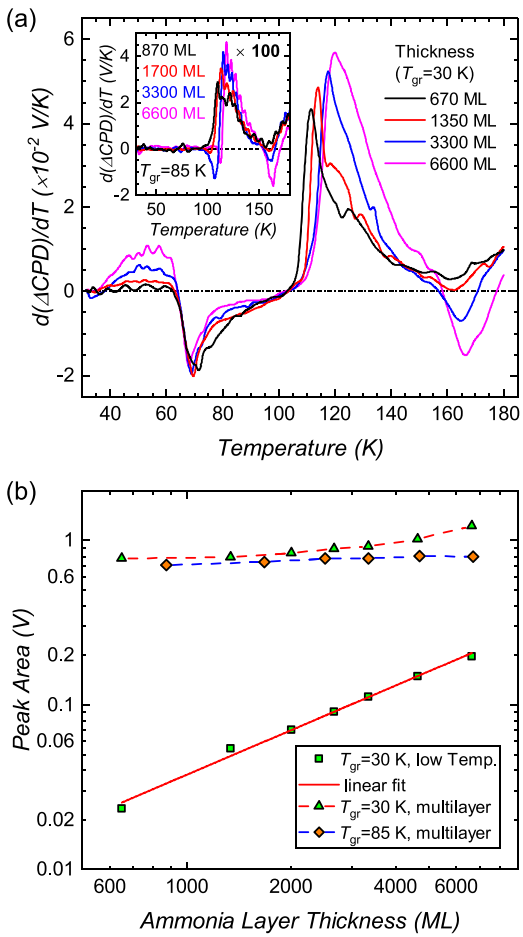

FIG. 6. Film thickness effect on the spontaneous polarization of solid ammonia films. (a) d(ΔCPD)/dT spectra of 670 ML–6600 ML-thick ammonia films grown at 30 K and at 85 K (inset). (b) The corresponding area under the low-temperature peak (filled squares) and that of the multilayer (filled triangles and diamonds for films grown at 30 K and 85 K, respectively). The low-temperature peak uptake reveals a linear correlation with the thickness, L ($\Delta CPD = aL^b$, best fit gives $b = 0.95 \pm 0.10$). The log–log scale emphasizes the power correlation since the exponent is equal to the slope of the linear line.

on the heating rate. In their work, Zheng and Kaiser annealed the films at a heating rate of ~0.008 K/s, 125 times slower than the rate used here. This may explain the difference between the crystallization temperature of 57 K that these authors and 65 K reported here. Lower heating rates allow more time for the film to respond to the temperature ramp.[74] Our analysis is further supported by the fact that the peak temperature is thickness independent and thus also mass independent (see discussion below and Fig. S5 of the supplementary material).

Satorre *et al.*[37] have demonstrated by double laser interferometry that amorphous ammonia films are porous and their porosity changes with growth temperature. From their data, we could estimate the density of films grown at 30 K to be 0.76 ± 0.04 g/cm^3. They have shown that the density increases to 0.89 g/cm^3 at T_{gr} = 60 K. This value pertains to the compact film density, since it remains constant above 60 K. Hence, we attribute the Kr lowest-temperature desorption peak at 52 K to some structural modification, e.g., pore collapse and transition to a denser film. It cannot be associated with the Kr multilayer desorption, since the multilayer peak of an equivalent Kr coverage adsorbed on the bare Ru(0001) substrate is obtained at significantly lower temperatures [the second Kr monolayer desorbs at ~45 K;[48] see an example in Fig. S2(a) of the supplementary material]. This assignment is further supported by the growing amplitude of the corresponding d(ΔCPD)/dT peak with film thickness, while its temperature does not shift [Fig. 6(a)]. It is also supported by the absence of this low temperature ΔP-TPD peak when the Kr is adsorbed on top of the ammonia film grown at 50 K [see Fig. S2(b) of the supplementary material]. There, only the 65 K and 115 K peaks are observed. In this case, the 65 K desorption peak well correlates with a peak in the d(ΔCPD)/dT spectrum. Nevertheless, correlating the depolarization of ammonia films grown at T_{gr} below 65 K with morphology modifications, e.g., pore collapse, requires the identification of the markers (e.g. unique IR spectra) of solid ammonia surface molecules.

In contrast to water, where calculations assigning IR bands to surface sites[75] have proven to correspond to the acquired experimental data[76] and were found to correlate with the water depolarization upon heating,[77] similar IR markers for the case of thick ammonia films have not been fully identified so far. Dawes *et al.*[36] and Zheng and Kaiser[38] reported on several IR bands that change during annealing of amorphous ammonia films. Among them, a broad peak at ~1100 cm^{-1} (the ν_2 symmetric deformation) that upon crystallization to the cubic phase splits into three components (with some frequency disagreements between the two works). Dawes *et al.* correlated this band to molecules residing at the surface. If that is the case, this band may serve as a marker for both structural changes

and phase transition and may be compared to events recorded by TP-ΔCPD measurements, similar to the work conducted on water films by Bu *et al.*[77] In this context, it will be worthwhile to investigate to what extent the porosity of the ammonia films is sensitive to the growth conditions. It is well established that the porosity of ASW films is not only growth temperature dependent[78–82] but is also strongly affected by the growth rate[82] and by the incidence angle in the case of molecular beam deposition.[83] The latter approach can produce compact ASW films when the beam impinges at small angles of incidence with respect to the surface normal. The porosity increases with the incidence angle, where backfilling vapor deposition is considered to be equivalent to deposition at the averaged angle of 45°. If ammonia behaves similarly, it will allow the investigation of the presumed correlation between the surface markers and the film morphology independently of the growth temperature. Such investigation has not yet been performed.

Both groups above[36,38] have claimed that they identified a "thermal memory" of the ammonia films based on their observations that films grown at elevated temperatures maintained their IR-absorbance profiles after cooling to 10 K. Furthermore, IR spectra of amorphous films that were grown at a low temperature and were subsequently annealed to T_{ann} did not resemble those of films grown at T_{ann}. It was suggested that the annealing of the amorphous films leads to their densification and eventually to their crystallization, however with a distribution of crystalline grains of different sizes. This distribution is assumed to differ from that of a film initially grown at T_{ann}, thus in our study has led to different TP-ΔCPD profiles.

Given the grain size distribution hypothesis, the observed variations in the TP-ΔCPD and the d(ΔCPD)/dT profiles may explain why these curves do not overlap until the monolayer desorption. They show profile variations that can be observed also during the multilayer desorption [e.g., curves (e) and (f) of Fig. 4(b)]. This indicates that their morphology is distinguished even following pores' collapse. The growth temperature does not determine only the films' initial morphology but also the morphology obtained following the films' reconstruction. Additionally, identification of the crystallization onset temperature demonstrates that ammonia forms spontaneous polarization even in the crystalline (also compact) phase, as seen in Fig. 3 for films grown at T_{gr} above 65 K.

D. Film thickness effect

The correlation between the desorption of Kr atoms from surface sites and the depolarization of the amorphous films (films grown below 65 K), both occurring during annealing, have led us to the conclusion that the depolarization process observed at low temperatures is attributed to surface reconstruction due to the collapse of the porous matrix. The multilayer desorption at 115 K is, however, responsible for the most significant depolarization seen at all films, i.e., most of the polarization is kept within the multilayer matrix of the film. The contribution of the surface area to the spontaneous polarization can be further investigated by varying the film thickness, since the surface area of a film with a uniform porosity linearly increases with the thickness. TP-ΔCPD measurements and their temperature derivative can differentiate between the contributions of dipole accumulation in the bulk and that of the surface dipoles. The first should be manifested by modifications of the multilayer desorption peak, which is expected to follow zero-order kinetics, and thus, it should slightly shift to higher temperatures as the thickness increases. Its effect on the intensity is expected to be weak due to the low level of polarization seen. If the dipoles have a component normal to the substrate, then the intensity is expected to increase. If their orientation is random, we should see only the contribution of the first (bottommost) 30 layers responsible for the −3.4 V minimum measured during the film growth. Changing the surface area should, therefore, affect the low temperature features. In that case, the d(ΔCPD)/dT peak temperature is expected to remain in place if the voltage develops linearly with the surface area, as Bu *et al.*[77] have shown in the case of water.

Figure 6 demonstrates the thickness effect on the d(ΔCPD)/dT spectra for films grown at 30 K and 85 K [Fig. 6(a) and its inset]. Common to both growth temperatures is that by increasing the film thickness, a shift of the multilayer desorption peak to higher temperatures takes place. It is associated with growing amplitudes, demonstrating zero-order kinetics [Fig. S4(b) of the supplementary material] with an apparent sublimation energy of 2.8 ± 0.2 kcal/mol, in agreement with previous calculations of the hydrogen-bond strength in ammonia ice I.[28] The low-temperature feature observed for films grown at 30 K reveals a strong dependence on the film thickness. Indeed, the depolarization/reconstruction process observed between 30 K and 65 K demonstrates a first order-like kinetics; the peak temperature remains unchanged (see also Fig. S5 of the supplementary material) and the contact potential difference linearly increases with the thickness [best fit to $\Delta CPD = aL^b$ shows a power law behavior with b = 0.95 ± 0.10; Fig. 6(b)]. This behavior does not occur in films grown at T_{gr} = 85 K, where no low-temperature peak evolves, i.e., no structural rearrangement is recognized below the desorption of the multilayer. The curves in Fig. 6(b) further demonstrate that the polarization changes during film reconstruction are affected the most by the film thickness. The voltage difference due to the pore collapse increases 10-fold between films of 670 ML and 6600 ML, while the area of the multilayer desorption peak is affected relatively much less. At the same time, however, the multilayer's contribution to the voltage is still significantly larger in both films grown at 30 K and 85 K.

IV. CONCLUSIONS

Due to the limited information on the behavior of thick solid ammonia films, particularly in comparison to water, we have performed several characterizations in order to fill some of the relevant knowledge gaps. Among those, we have shown that adsorbed ammonia molecules can compress and cage other coadsorbed atoms/molecules, resulting from their strong interaction with the substrate. This is a well-documented phenomenon observed in the case of water. These together with IR measurements reported in the literature allowed us to associate features in the TP-ΔCPD profiles and their temperature derivative to phase transition and structural rearrangements. By employing continuous contact potential difference measurements utilizing *in situ* non-invasive Kelvin probe, we have shown that the spontaneous polarization of thick solid ammonia films, either amorphous or crystalline, has a prominent temperature dependence. This is manifested by two processes: the effect of growth temperature and the consequence of film annealing.

The growth reveals three distinguished trends at different temperature regimes. These trends include varying degrees of polarization and even a net (average) polarization flipping. The overall measured ΔCPD during growth has contributions from the initial "short range" interaction of the adsorbate with the substrate and a "long range" contribution of the net macroscopic dipole alignment. The first is responsible for most of the measured ΔCPD and was found to be much stronger in ammonia than in water (−1.75 V and −3.4 V ΔCPD for water and ammonia, respectively). In addition, this interaction is growth temperature independent. This is also evident in the TP-ΔCPD profiles, where most of the ΔCPD evolved during growth diminishes during the monolayer desorption. At higher coverages, the film polarization originates from a net macroscopic dipole alignment that leads to electric field evolution across the film. Overall, thick solid ammonia films have a weaker dipole interaction/alignment than water and, consequently, a weaker temperature dependence, except for the narrow growth temperature range of 60 K–75 K, where significant modifications were observed. We assign ammonia to the family of materials classified as "spontelectrics" due to the similar temperature dependence they exhibit (memory of their "thermal history") that affects the internal electric field.

We have shown indications that film reconstruction and crystallization upon annealing occur in the temperature range of 50 K–65 K. We conclude that the varied film morphology, governed by the growth temperature and manifested by the spontaneous evolution of polarization, well-correlates with the IR observations as a function of temperature reported in the literature. We have provided more evidence for the films' thermal "memory" effect based on temperature dependent depolarization measurements, derived from the fact that films grown at different temperatures have a unique depolarization pathway. This was demonstrated by ΔP-TPD of Kr atoms embedded within the ammonia film, which were employed as an internal probe of the film structure/porosity during its annealing.

We conclude with a general statement that characterization by contact potential difference with the appropriate temperature control can be utilized non-invasively to monitor morphology modifications and phase transitions, at least for solids of polar molecules, as was demonstrated here for solid ammonia.

SUPPLEMENTARY MATERIAL

See the supplementary material for supporting data concerning the similarity between ΔP-TPD and d(ΔCPD)/dT spectra of ammonia films, ΔP-TPD profiles of thin methyl chloride and Kr films adsorbed directly on the Ru(0001) surface and Kr atoms adsorbed on thick solid ammonia film, both grown at 50 K, utilized as a probe for identifying peaks observed in the TP-ΔCPD and d(ΔCPD)/dT spectra, data regarding the monolayer contribution to the overall measured ΔCPD, as it is reflected in a typical full temperature-scale TP-ΔCPD profile, analysis of the film thickness effect, including isothermal desorption curves and the film thickness-multilayer desorption–peak correlation, both demonstrating the multilayer zero-order kinetics, and detailed data and calculations concerning the spontaneous polarization, mostly the electric fields developed within the ammonia films and dipole orientation.

ACKNOWLEDGMENTS

Partial support by the Israel Science Foundation (ISF, Grant No. 52/14) and by the German-Israeli Foundation (GIF) is acknowledged. The critical technical support provided by Dr. Eduard Mastov, Marcelo Friedman, Shaul Binyamini, and Alexander Lantsman is greatly appreciated.

DATA AVAILABILITY

The data that supports the findings of this study are available within the article and its supplementary material.

REFERENCES

[1] A. C. A. Boogert, P. A. Gerakines, and D. C. B. Whittet, "Observations of the icy universe," Annu. Rev. Astron. Astrophys. **53**, 541–581 (2015).
[2] P. T. P. Ho and C. H. Townes, "Interstellar ammonia," Annu. Rev. Astron. Astrophys. **21**, 239–270 (1983).
[3] J. Jijina, P. C. Myers, and F. C. Adams, "Dense cores mapped in ammonia: A database," Astrophys. J. Suppl. Ser. **125**, 161 (1999).
[4] J. P. Emery, D. M. Burr, D. P. Cruikshank, R. H. Brown, and J. B. Dalton, "Near-infrared (0.8–4.0 μm) spectroscopy of Mimas, Enceladus, Tethys, and Rhea," Astron. Astrophys. **435**, 353–362 (2005).
[5] J. Bauer, T. L. Roush, T. R. Geballe, K. J. Meech, T. C. Owen, W. D. Vacca, J. T. Rayner, and K. T. C. Jim, "The near infrared spectrum of Miranda: Evidence of crystalline water ice," Icarus **158**, 178–190 (2002).
[6] W. M. Grundy, R. P. Binzel, B. J. Buratti, J. C. Cook, D. P. Cruikshank, C. M. Dalle Ore, A. M. Earle, K. Ennico, C. J. A. Howett, A. W. Lunsford, C. B. Olkin, A. H. Parker, S. Philippe, S. Protopapa, E. Quirico, D. C. Reuter, B. Schmitt, K. N. Singer, A. J. Verbiscer, R. A. Beyer, M. W. Buie, A. F. Cheng, D. E. Jennings, I. R. Linscott, J. W. Parker, P. M. Schenk, J. R. Spencer, J. A. Stansberry, S. A. Stern, H. B. Throop, C. C. C. Tsang, H. A. Weaver, G. E. Weigle, L. A. Young, and New Horizons Science Team, "Surface compositions across Pluto and Charon," Science **351**, aad9189 (2016).
[7] C. M. D. Ore, D. P. Cruikshank, S. Protopapa, F. Scipioni, W. B. McKinnon, J. C. Cook, W. M. Grundy, B. Schmitt, S. A. Stern, J. M. Moore, A. Verbiscer, A. H. Parker, K. N. Singer, O. M. Umurhan, H. A. Weaver, C. B. Olkin, L. A. Young, and K. Ennico, "Detection of ammonia on Pluto's surface in a region of geologically recent tectonism," Sci. Adv. **5**, eaav5731 (2019).
[8] S. K. Atreya, P. R. Mahaffy, H. B. Niemann, M. H. Wong, and T. C. Owen, "Composition and origin of the atmosphere of Jupiter—An update, and implications for the extrasolar giant planets," Planet. Space Sci. **51**, 105–112 (2003).
[9] M. Hofstadter, "Latitudinal variations of ammonia in the atmosphere of Uranus: An analysis of microwave observations," Icarus **81**, 396–412 (1989).
[10] J. Joiner, P. G. Steffes, and J. M. Jenkins, "Laboratory measurements of the 7.5–9.38 mm absorption of gaseous ammonia (NH_3) under simulated jovian conditions," Icarus **81**, 386–395 (1989).
[11] O. Grasset, C. Sotin, and F. Deschamps, "On the internal structure and dynamics of Titan," Planet. Space Sci. **48**, 617–636 (2000).
[12] M. E. Brown and W. M. Calvin, "Evidence for crystalline water and ammonia ices on Pluto's satellite Charon," Science **287**, 107–109 (2000).
[13] J. H. Waite, "Cassini ion and neutral mass spectrometer: Enceladus plume composition and structure," Science **311**, 1419–1422 (2006).
[14] M. J. Mumma and S. B. Charnley, "The chemical composition of comets—Emerging taxonomies and natal heritage," Annu. Rev. Astron. Astrophys. **49**, 471–524 (2011).
[15] H. Wang, R. C. Bell, M. J. Iedema, A. A. Tsekouras, and J. P. Cowin, "Sticky ice grains aid planet formation: Unusual properties of cryogenic water ice," Astrophys. J. **620**, 1027–1032 (2005).
[16] C. R. Hill, D. Heißelmann, J. Blum, and H. J. Fraser, "Collisions of small ice particles under microgravity conditions," Astron. Astrophys. **573**, A49 (2015).

[17]A. Rosu-Finsen, J. Lasne, A. Cassidy, M. R. S. McCoustra, and D. Field, "Enabling star formation via spontaneous molecular dipole orientation in icy solids," Astrophys. J. **832**, 1 (2016).
[18]A. Lafosse, M. Bertin, A. Domaracka, D. Pliszka, E. Illenberger, and R. Azria, "Reactivity induced at 25 K by low-energy electron irradiation of condensed NH_3–CH_3COOD (1:1) mixture," Phys. Chem. Chem. Phys. **8**, 5564–5568 (2006).
[19]M. Bertin, I. Martin, F. Duvernay, P. Theule, J. B. Bossa, F. Borget, E. Illenberger, A. Lafosse, T. Chiavassa, and R. Azria, "Chemistry induced by low-energy electrons in condensed multilayers of ammonia and carbon dioxide," Phys. Chem. Chem. Phys. **11**, 1838 (2009).
[20]D. P. Zaleski, N. A. Seifert, A. L. Steber, M. T. Muckle, R. A. Loomis, J. F. Corby, O. Martinez, K. N. Crabtree, P. R. Jewell, J. M. Hollis, F. J. Lovas, D. Vasquez, J. Nyiramahirwe, N. Sciortino, K. Johnson, M. C. McCarthy, A. J. Remijan, and B. H. Pate, "Detection of E-Cyanomethanimine toward Sagittarius B2(N) in the Green Bank Telescope PRIMOS survey," Astrophys. J. **765**, L10 (2013).
[21]K. Altwegg, H. Balsiger, A. Bar-Nun, J. J. Berthelier, A. Bieler, P. Bochsler, C. Briois, U. Calmonte, M. R. Combi, H. Cottin, J. De Keyser, F. Dhooghe, B. Fiethe, S. A. Fuselier, S. Gasc, T. I. Gombosi, K. C. Hansen, M. Haessig, A. Jäckel, E. Kopp, A. Korth, L. Le Roy, U. Mall, B. Marty, O. Mousis, T. Owen, H. Rème, M. Rubin, T. Sémon, C. Y. Tzou, J. Hunter Waite, and P. Wurz, "Prebiotic chemicals-amino acid and phosphorus-in the coma of comet 67P/Churyumov-Gerasimenko," Sci. Adv. **2**, e1600285 (2016).
[22]K. I. Öberg, "Photochemistry and astrochemistry: Photochemical pathways to interstellar complex organic molecules," Chem. Rev. **116**, 9631–9663 (2016).
[23]C. R. Arumainayagam, R. T. Garrod, M. C. Boyer, A. K. Hay, S. T. Bao, J. S. Campbell, J. Wang, C. M. Nowak, M. R. Arumainayagam, and P. J. Hodge, "Extraterrestrial prebiotic molecules: Photochemistry vs radiation chemistry of interstellar ices," Chem. Soc. Rev. **48**, 2293–2314 (2019).
[24]J. C. Cook, S. J. Desch, T. L. Roush, C. A. Trujillo, and T. R. Geballe, "Near-infrared spectroscopy of Charon: Possible evidence for cryovolcanism on Kuiper belt objects," Astrophys. J. **663**, 1406–1419 (2007).
[25]M. Neveu, S. J. Desch, and J. C. Castillo-Rogez, "Aqueous geochemistry in icy world interiors: Equilibrium fluid, rock, and gas compositions, and fate of antifreezes and radionuclides," Geochim. Cosmochim. Acta **212**, 324–371 (2017).
[26]N. Uras, V. Buch, and J. P. Devlin, "Hydrogen bond surface chemistry: Interaction of NH_3 with an ice particle," J. Phys. Chem. B **104**, 9203–9209 (2000).
[27]Y. Liu and M. E. Tuckerman, "Protonic defects in hydrogen bonded liquids: Structure and dynamics in ammonia and comparison with water," J. Phys. Chem. B **105**, 6598–6610 (2001).
[28]A. D. Fortes, J. P. Brodholt, I. G. Wood, and L. Vočadlo, "Hydrogen bonding in solid ammonia from *ab initio* calculations," J. Chem. Phys. **118**, 5987–5994 (2003).
[29]J. Stähler, U. Bovensiepen, M. Meyer, and M. Wolf, "A surface science approach to ultrafast electron transfer and solvation dynamics at interfaces," Chem. Soc. Rev. **37**, 2180–2190 (2008).
[30]J. Stähler, M. Meyer, U. Bovensiepen, and M. Wolf, "Solvation dynamics of surface-trapped electrons at NH_3 and D_2O crystallites adsorbed on metals: From femtosecond to minute timescales," Chem. Sci. **2**, 907 (2011).
[31]R. Sagi, M. Akerman, S. Ramakrishnan, and M. Asscher, "The role of thermal history on spontaneous polarization and phase transitions of amorphous solid water films studied by contact potential difference measurements" (submitted) (2020).
[32]K. Kutzner, "Spontaneous polarization of condensing carbon monoxide and other gases with an electrical dipole moment," Thin Solid Films **14**, 49–61 (1972).
[33]A. Cassidy, R. L. James, A. Dawes, and D. Field, *Crystallites and Electric Fields in Solid Ammonia* (ChemistryOpen, 2020).
[34]J. R. Ferraro, G. Sill, and U. Fink, "Infrared intensity measurements of cryodeposited thin films of NH_3, NH_4HS, H_2S, and assignments of absorption bands," Appl. Spectrosc. **34**, 525 (2016).
[35]B. M. Giuliano, R. Martín-Doménech, R. M. Escribano, J. Manzano-Santamaría, and G. M. Muñoz Caro, "Interstellar ice analogs: H_2O ice mixtures with CH_3OH and NH_3 in the far-IR region," Astron. Astrophys. **592**, A81 (2016).
[36]A. Dawes, R. J. Mukerji, M. P. Davis, P. D. Holtom, S. M. Webb, B. Sivaraman, S. V. Hoffmann, D. A. Shaw, and N. J. Mason, "Morphological study into the temperature dependence of solid ammonia under astrochemical conditions using vacuum ultraviolet and Fourier-transform infrared spectroscopy," J. Chem. Phys. **126**, 244711 (2007).
[37]M. Á. Satorre, J. Leliwa-Kopystynski, C. Santonja, and R. Luna, "Refractive index and density of ammonia ice at different temperatures of deposition," Icarus **225**, 703–708 (2013).
[38]W. Zheng and R. I. Kaiser, "An infrared spectroscopy study of the phase transition in solid ammonia," Chem. Phys. Lett. **440**, 229–234 (2007).
[39]C. Benndorf and T. E. Madey, "Adsorption and orientation of NH_3 on Ru(001)," Surf. Sci. **135**, 164–183 (1983).
[40]G. B. Fisher, "The electronic structure of two forms of molecular ammonia adsorbed on Pt(111)," Chem. Phys. Lett. **79**, 452–458 (1981).
[41]Z. Rosenzweig and M. Asscher, "Optical second-harmonic generation from surfaces as a monitor for adsorbate induced work function changes," Surf. Sci. **204**, L732–L738 (1988).
[42]T. Livneh and M. Asscher, "The adsorption and decomposition of C_2H_4 on Ru(001): A combined tpr and work function change study," J. Phys. Chem. B **104**, 3355–3363 (2000).
[43]H. A. Engelhardt, P. Feulner, H. Pfnür, and D. Menzel, "An accurate and versatile vibrating capacitor for surface and adsorption studies," J. Phys. E: Sci. Instrum. **10**, 1133 (1977).
[44]H. Pfnür and D. Menzel, "The influence of adsorbate interactions on kinetics and equilibrium for CO on Ru(001). I. Adsorption kinetics," J. Chem. Phys. **79**, 2400–2410 (1983).
[45]H. Pfnür, P. Feulner, and D. Menzel, "The influence of adsorbate interactions on kinetics and equilibrium for CO on Ru(001). II. Desorption kinetics and equilibrium," J. Chem. Phys. **79**, 4613–4623 (1983).
[46]Y. Lilach, L. Romm, T. Livneh, and M. Asscher, "The first layers of water on Ru(001)," J. Phys. Chem. B **105**, 2736–2742 (2001).
[47]T. Livneh, Y. Lilach, and M. Asscher, "Dipole–dipole interactions among CH_3Cl molecules on Ru(001): Correlation between work function change and thermal desorption studies," J. Chem. Phys. **111**, 11138–11146 (1999).
[48]H. Schlichting and D. Menzel, "Techniques for attainment, control, and calibration of cryogenic temperatures at small single-crystal samples under ultrahigh vacuum," Rev. Sci. Instrum. **64**, 2013–2022 (1993).
[49]D. L. Doering and T. E. Madey, "The adsorption of water on clean and oxygen-dosed Ru(001)," Surf. Sci. **123**, 305–337 (1982).
[50]G. Held and D. Menzel, "Isotope effects in structure and kinetics of water adsorbates on Ru(001)," Surf. Sci. **327**, 301–320 (1995).
[51]D. N. Denzler, S. Wagner, M. Wolf, and G. Ertl, "Isotope effects in the thermal desorption of water from Ru(001)," Surf. Sci. **532-535**, 113–119 (2003).
[52]T. E. Madey, J. E. Houston, C. W. Seabury, and T. N. Rhodin, "The structure of NH_3 on Ni(111)," J. Vac. Sci. Technol. **18**, 476–480 (1981).
[53]Z. Rosenzweig and M. Asscher, "Interaction of NH_3 with Re(0001): An optical second harmonic generation study," Surf. Sci. **225**, 249–259 (1990).
[54]M. C. Wu, C. M. Truong, and D. W. Goodman, "Interactions of ammonia with a nickel oxide (100) surface studied by high-resolution electron energy loss spectroscopy and temperature programmed desorption spectroscopy," J. Phys. Chem. **97**, 4182–4186 (1993).
[55]R. M. van Hardeveld, R. A. van Santen, and J. W. Niemantsverdriet, "The adsorption of NH_3 on Rh(111)," Surf. Sci. **369**, 23–35 (1996).
[56]S. Maier, I. Stass, J. I. Cerda, and M. Salmeron, "Bonding of ammonia and its dehydrogenated fragments on Ru(0001)," J. Phys. Chem. C **116**, 25395–25400 (2012).
[57]Y. Zhou, S. Akhter, and J. M. White, "The adsorption of ammonia on Ru(001) and its effect on coadsorbed CO," Surf. Sci. **202**, 357–376 (1988).
[58]Y. Lilach and M. Asscher, "Compression and caging of CD_3Cl by H_2O layers on Ru(001)," J. Chem. Phys. **117**, 6730–6736 (2002).
[59]T. Livneh, L. Romm, and M. Asscher, "Cage formation of N_2 under H_2O overlayer on Ru(001)," Surf. Sci. **351**, 250–258 (1996).
[60]R. S. Smith, C. Huang, E. K. L. Wong, and B. D. Kay, "The molecular volcano: Abrupt CCl_4 desorption driven by the crystallization of amorphous solid water," Phys. Rev. Lett. **79**, 909–912 (1997).

[61] B. L. Maschhoff and J. P. Cowin, "Corrected electrostatic model for dipoles adsorbed on a metal surface," J. Chem. Phys. **101**, 8138–8151 (1994).
[62] S. Maier, B. A. J. Lechner, G. A. Somorjai, and M. Salmeron, "Growth and structure of the first layers of ice on Ru(0001) and Pt(111)," J. Am. Chem. Soc. **138**, 3145–3151 (2016).
[63] C. P. Smyth and C. S. Hitchcock, "The dielectric constants and transitions of solid ammonia, hydrogen sulfide and methyl alcohol," J. Am. Chem. Soc. **56**, 1084–1087 (1934).
[64] P. V. Hobbs, *Ice Physics* (Clarendon Press, Oxford, UK, 1974).
[65] H. Wang, R. C. Bell, M. J. Iedema, G. K. Schenter, K. Wu, and J. P. Cowin, "Pyroelectricity of water ice," J. Phys. Chem. B **112**, 6379–6389 (2008).
[66] A. W. Hewat and C. Riekel, "The crystal structure of deuteroammonia between 2 and 180 K by neutron powder profile refinement," Acta Crystallogr., Sect. A **35**, 569–571 (1979).
[67] C. Kittel, *Introduction to Solid State Physics*, 8th ed. (Wiley, New York, 2005).
[68] Y. H. Zhao, M. H. Abraham, and A. M. Zissimos, "Fast calculation of van der Waals volume as a sum of atomic and bond contributions and its application to drug compounds," J. Org. Chem. **68**, 7368–7373 (2003).
[69] D. D. Kemp and M. S. Gordon, "An interpretation of the enhancement of the water dipole moment due to the presence of other water molecules," J. Phys. Chem. A **112**, 4885–4894 (2008).
[70] A. Natan, L. Kronik, H. Haick, and R. T. Tung, "Electrostatic properties of ideal and non-ideal polar organic monolayers: Implications for electronic devices," Adv. Mater. **19**, 4103–4117 (2007).
[71] O. Plekan, A. Cassidy, R. Balog, N. C. Jones, and D. Field, "Spontaneous electric fields in films of *cis*-methyl formate," Phys. Chem. Chem. Phys. **14**, 9972 (2012).
[72] J. Stähler, M. Meyer, D. O. Kusmierek, U. Bovensiepen, and M. Wolf, "Ultrafast electron transfer dynamics at NH_3/Cu(111) interfaces: Determination of the transient tunneling barrier," J. Am. Chem. Soc. **130**, 8797–8803 (2008).
[73] D. Field, O. Plekan, A. Cassidy, R. Balog, N. C. Jones, and J. Dunger, "Spontaneous electric fields in solid films: Spontelectrics," Int. Rev. Phys. Chem. **32**, 345–392 (2013).
[74] N. J. Sack and R. A. Baragiola, "Sublimation of vapor-deposited water ice below 170 K, and its dependence on growth conditions," Phys. Rev. B **48**, 9973–9978 (1993).
[75] V. Buch and J. P. Devlin, "Spectra of dangling OH bonds in amorphous ice: Assignment to 2- and 3-coordinated surface molecules," J. Chem. Phys. **94**, 4091–4092 (1991).
[76] B. Rowland and J. P. Devlin, "Spectra of dangling OH groups at ice cluster surfaces and within pores of amorphous ice," J. Chem. Phys. **94**, 812–813 (1991).
[77] C. Bu, J. Shi, U. Raut, E. H. Mitchell, and R. A. Baragiola, "Effect of microstructure on spontaneous polarization in amorphous solid water films," J. Chem. Phys. **142**, 134702 (2015).
[78] A. Bar-Nun, I. Kleinfeld, and E. Kochavi, "Trapping of gas mixtures by amorphous water ice," Phys. Rev. B **38**, 7749–7754 (1988).
[79] E. Mayer and R. Pletzer, "Astrophysical implications of amorphous ice- a microporous solid," Nature **319**, 298–301 (1986).
[80] G. A. Kimmel, K. P. Stevenson, Z. Dohnálek, R. S. Smith, and B. D. Kay, "Control of amorphous solid water morphology using molecular beams. I. Experimental results," J. Chem. Phys. **114**, 5284–5294 (2001).
[81] D. E. Brown, S. M. George, C. Huang, E. K. L. Wong, K. B. Rider, R. S. Smith, and B. D. Kay, "H_2O condensation coefficient and refractive index for vapor-deposited ice from molecular beam and optical interference measurements," J. Phys. Chem. **100**, 4988–4995 (1996).
[82] B. S. Berland, D. E. Brown, M. A. Tolbert, and S. M. George, "Refractive index and density of vapor-deposited ice," Geophys. Res. Lett. **22**, 3493–3496, https://doi.org/10.1029/95gl03504 (1995).
[83] K. P. Stevenson, G. A. Kimmel, Z. Dohnálek, R. S. Smith, and B. D. Kay, "Controlling the morphology of amorphous solid water," Science **283**, 1505–1507 (1999).